Cellular/Molecular

Different Mechanisms Promote Astrocyte Ca^{2+} Waves and Spreading Depression in the Mouse Neocortex

Oliver Peters,[1] Carola G. Schipke,[1] Yoshinori Hashimoto,[2] and Helmut Kettenmann[1]

[1]Max-Delbrück Center for Molecular Medicine, Cellular Neuroscience, D-13092 Berlin, Germany, and [2]Laboratory of Cellular Neurobiology, Tokyo University of Pharmacy & Life Science, Hachioji, Tokyo 192-0392, Japan

Cortical spreading depression (CSD) is thought to play an important role in different pathological conditions of the human brain. Here we investigated the interaction between CSD and Ca^{2+} waves within the astrocyte population in slices from mouse neocortex (postnatal days 10–14). After local KCl ejection as a trigger for CSD, we recorded the propagation of Ca^{2+} increases within a large population of identified astrocytes in synchrony with CSD measured as intrinsic optical signal (IOS) or negative DC-potential shift. The two events spread with 39.2 ± 3.3 μm/sec until the IOS and negative DC-potential shift decayed after ~1 mm. However, the astrocyte Ca^{2+} wave continued to propagate for up to another 500 μm but with a reduced speed of 18.3 ± 2.5 μm/sec that is also typical for glial Ca^{2+} waves in white matter or culture. While blocking CSD using MK-801 (40 μM), an NMDA-receptor antagonist, the astrocyte Ca^{2+} wave persisted with a reduced speed (13.2 ± 1.5 μm/sec). The specific gap junction blocker carbenoxolon (100 μM) did not prevent CSD but decelerated the speed (2.9 ± 0.9 μm/sec) of the astrocyte Ca^{2+} wave in the periphery of CSD. We also found that interfering with intracellular astrocytic Ca^{2+} signaling by depletion of internal Ca^{2+} stores does not affect the spread of the IOS. We conclude that CSD determines the velocity of an accompanying astrocytic Ca^{2+} response, but the astrocyte Ca^{2+} wave penetrates a larger territory and by this represents a self-reliant phenomenon with a different mechanism of propagation.

Key words: **glia; neocortex; gap junctions; intrinsic optical signals; migraine; stroke**

Introduction

Cortical spreading depression (CSD) is classically defined as a slowly propagating wave (30–50 μm/sec) of neuronal depolarization in the mammalian brain (Leao, 1944). Over the recent years, the clinical impact of CSD has become more and more obvious (for review, see Gorji, 2001). CSD has been recognized to cause the aura of migraine in human (Lauritzen, 1994; Hadjikhani et al., 2001) and may play a role in the progression of cortical infarct volume after stroke (Iijima et al., 1992; Back et al., 1996). The cellular mechanisms of initiation and propagation of CSD are still poorly understood. Several lines of evidence have led to the speculation that astrocytes may carry the propagating wave front of CSD (Martins-Ferreira et al., 2000), but studies focused on inter-astrocytic signaling in CSD were lacking so far.

Communication between astrocytes in response to a local stimulus is achieved by the intercellular propagation of increases in the cytosolic Ca^{2+} concentration $[Ca^{2+}]_i$ (Verkhratsky and Kettenmann, 1996; Araque et al., 2001). Propagation of transient Ca^{2+} increases through a layer of astrocytes has first been observed in cell culture, and this wave of activity spreads slower than CSD, with a velocity of ~20 μm/sec (Cornell-Bell et al., 1990; Dani et al., 1992). Astrocytic Ca^{2+} waves were for a long time considered as the *in vitro* correlate of CSD, but recently, spreading Ca^{2+} increases within the astrocytic network have also been observed *in situ*, namely in the retina (Newman and Zahs, 1997) and in the corpus callosum (Schipke et al., 2002). Astrocyte Ca^{2+} waves propagate either mediated by ATP release and subsequent activation of purinergic receptors (Guthrie et al., 1999; Cotrina et al., 2000; Stout et al., 2002) or gap junctions (Charles, 1998; Giaume and Venance, 1998). Interestingly, several gap junction blockers have been shown to prevent the propagation of spreading depression (SD) (Nedergaard et al., 1995), suggesting a leading role for astrocytes in CSD. In contrast, it was reported recently that astrocyte-directed inactivation of connexin 43, the most prominent component of astrocytic gap junctions, accelerates spreading depression (Theis et al., 2003). Studies with the aim to elucidate the role of intracellular Ca^{2+} increases for the propagation of CSD led to controversial results. Basarsky et al. (1998) demonstrated that Ca^{2+} waves in the hippocampus, in which single astrocytes were shown to participate, were not required for its propagation. In contrast, in hippocampal organ cultures, SD and intercellular Ca^{2+} waves could not be separated (Kunkler and Kraig, 1998).

In the present study, we combined different imaging and electrophysiological methods to both monitor wide-range signaling and cellular responses on the single-cell level. We were able to visualize Ca^{2+} transients from a large population of individual astrocytes in the neocortical network. Our technique allowed to study the interaction of CSD and astrocyte Ca^{2+} signaling in acute slices of the neocortex. We are able to show that CSD promotes the astrocytic Ca^{2+} wave, but that the astrocyte signal can

Received July 17, 2003; revised Sept. 5, 2003; accepted Sept. 5, 2003.

This work was supported by Deutsche Forschungsgemeinschaft Sonderforschungsbereich 515.

Correspondence should be addressed to Dr. Helmut Kettenmann, Max-Delbrück-Center for Molecular Medicine, Robert-Rössle-Strasse 10, 13092 Berlin, Germany. E-mail: hketten@mdc-berlin.de.

 0270-6474/03/239888-09$15.00/0

also spread independently, indicating that different mechanisms of propagation underlie the two events.

Materials and Methods

Animals, preparation of brain slices, and calcium recordings. For slice preparation, postnatal day 10 (P10) to P14 mice [either GFAP/enhanced green fluorescent protein (EGFP) transgenic FVB/N mice or nontransgenic FVB/N and NMRI mice] were decapitated, and their brains were removed. We cut frontal slices of 250–300 μm thickness in ice-cold bicarbonate buffer using a vibratome (VT 1000 S; Leica, Heidelberg, Germany). Slices were stored at room temperature in gassed buffer for at least 45 min before staining. Slices were incubated with the Ca^{2+} indicator dyes Fluo-4 AM (10 μM; Molecular Probes, Eugene, OR) or X-Rhod AM (10 μM; Molecular Probes) in bicarbonate buffer for 30–45 min at room temperature. Slices were transferred to a perfusion chamber on an upright microscope (Axioskop FS; Zeiss, Oberkochen, Germany) and fixed in the chamber using a U-shaped platinum wire with a grid of nylon threads. Slices were superfused with gassed bicarbonate buffer at a flow rate of 4–6 ml/min and a temperature of 33–34°C. Substances were applied by changing the perfusate. Intracellular Ca^{2+} changes were detected using a cooled CCD camera (SensiCam; PCO, Kelheim, Germany). As a light source for fluorophore excitation, we used a monochromator set to the appropriate wavelength (T.I.L.L. Photonics, München, Germany). Intrinsic optical signals (IOS) were recorded as light transmittance with the same camera device as used for Ca^{2+} measurements. Slices were illuminated by long-pass-filtered white light (750 FH 90; Andover, Salem, MA). The light source for IOS was controlled using a personal computer (PC)-driven shutter. Images were stored on a PC and processed with conventional software (Image Pro; Media Cybernetics, Silver Spring, MD). For better illustrating the moving front of a Ca^{2+} wave and the corresponding IOS in measurements performed with low magnification (10× objective), we subtracted the image before stimulation from any given image on the basis of the pixel values. This procedure results in a series of images, which highlights only those regions that have changed after stimulation and thus shows only the responding cells. To elicit CSD, a small amount (~ 10 nl) of high-molar KCl (3 M) was ejected from a micropipette. The tip of the pipette was placed on top of the slice, with the pipette only gently touching the upper cell layer. To avoid artifacts in terms of direct response to high K^+, the area of interest was placed at least 200 μm distant from the tip of the pipette, and, in addition, the K^+ solution was always ejected into the opposite direction of the inspected region (Fig. 1*A*). Before measurement and stimulation was started, bath perfusion was stopped.

Electrophysiological recordings. For recording membrane currents, the patch-clamp technique in the whole-cell configuration was used. Electrodes with a resistance of 4–6 MΩ were pulled and filled with pipette solution. Because cell somata were located ~10–30 μm underneath the slice surface, pressure was applied to the pipette while it was advanced toward the cell. Extracellular DC-potential recordings and membrane currents were recorded with conventional electronics and digitized using a PC and the TIDA software package (EPC 9-amplifier; HEKA Elektronik, Lambrecht/Pfalz, Germany).

Solutions and electrodes. The standard bath solution contained the following (in mM): 134 NaCl, 2.5 KCl, 2 $CaCl_2$, 1.3 $MgCl_2$, 26 $NaHCO_3$, 1.25 K_2HPO_4, and 10 glucose. By gassing the solutions with carbogen, the pH was adjusted to 7.4. The pipette solution for patch-clamp recordings contained the following (in mM): 130 KCl, 2 $MgCl_2$, 0.5 $CaCl_2$, 5 EGTA, and 10 mM HEPES. Ca^{2+} activity of the pipette solution was ~11 nM. All experiments were performed at 33–34°C. Recording and stimulation pipettes were fabricated from borosilicate capillaries (Hilgenberg, Malsfeld, Germany). Drugs were applied to the bath solution in the following concentrations (in μM): 40 MK-801 ((+)-5-methyl-10,11-dihydro-5H-dibenzo [a,d] cyclohepten-5,10-imine maleate), 100 carbenoxolon, 500 octanol, 20 thapsigargin, and 2000 EGTA.

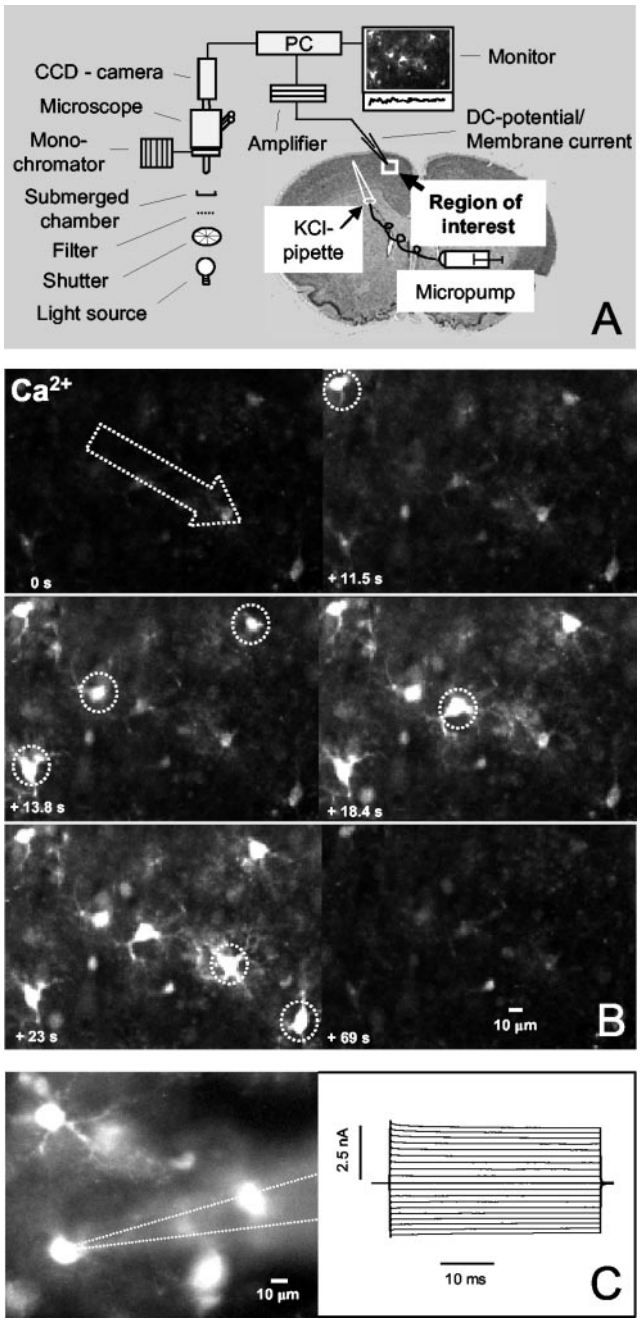

Figure 1. Ca^{2+} signals observed in neocortical astrocytes. *A*, A diagram of the experimental setup and the slice preparation placed in a submerged chamber. CSD was elicited by a focal release of KCl from a micropipette via a micropump. The white rectangle, situated in layers II–IV of the frontal cortex, denotes the observed region of interest. The fluorescence and IOS were recorded by a computer system (PC). Membrane currents or extracellular field potentials were measured, amplified, and transferred to a computer (PC). *B*, Ca^{2+} increases, measured as fluorescence changes in slices bulk loaded with the Ca^{2+} fluorescent dye Fluo-4, were recorded from the region of interest during CSD. The white dotted arrow indicates the direction in which CSD spreads. Dotted circles highlight cells that responded at the indicated time after stimulation. *C*, A cell responding with a fluorescence increase (left image) was approached with the patch pipette (dotted lines), and membrane currents were recorded. The membrane was clamped at − 80 mV and depolarized and hyperpolarized to −170 and +10 mV, respectively, with 10 mV increments. Note the passive membrane currents characteristic of astrocytes.

Results

CSD triggers a Ca^{2+} wave in identified astrocytes

We used a classical paradigm to elicit CSD by applying a small amount of high-molar KCl (3 M, ~10 nl) from a micropipette to the surface of a cortical slice. Slices had been bulk loaded with the fluorescent Ca^{2+} dyes X-Rhod AM or Fluo-4 AM to record Ca^{2+} signals. In parallel, we were able to measure the IOS as an indicator for the two-dimensional spread of CSD. Figure 1*A* is a dia-

gram of the experimental setup. As an instant response to KCl ejection, $[Ca^{2+}]_i$ increased in cells close to the stimulation pipette. Subsequently, cells more distant to the pipette responded with a Ca^{2+} signal. The delay correlated to the distance from the stimulation pipette, giving the impression of a Ca^{2+} wave spreading through a large population of single cells (Fig. 1*B*).

To study the cells, which responded with a Ca^{2+} increase during CSD, we imaged small areas in layers I–IV of the frontal neocortex (10× objective, 0.6 mm^2; 20×, 0.18 mm^2; or 40×, 0.04 mm^2), typically 300–500 μm away from the ejection pipette. We can exclude that the propagating wave is caused by a propagating $[K^+]$ increase in the bath attributable to the ejection of KCl from the pipette, because we were able to pharmacologically block the wave while still observing the Ca^{2+} response close to the KCl pipette (see below). We identified the Ca^{2+}-responsive cells by using several approaches. In the first approach, we imaged cells in slices from transgenic mice in which astrocytes are labeled by the expression of the EGFP (for details, see Nolte et al., 2001). Slices from these transgenic animals were bulk loaded with the Ca^{2+} indicator dye X-Rhod AM. Approximately 10% of the X-Rhod-stained cells were found to be EGFP-positive cells and thus identified as astrocytes. Because we know that EGFP is not expressed in all cortical astrocytes of this transgenic animal, we used an additional approach to identify the remainder population. The cells were characterized on the basis of their membrane current pattern using the patch-clamp technique. EGFP-negative, X-Rhod-stained cells (17 cells from 14 different slices) were clamped at −70 mV close to their resting potential. Depolarizing and hyperpolarizing current pulses were applied to clamp the membrane potentials ranging from −160 to +20 mV (10 mV increments). The resulting currents showed no time-dependent activation or inactivation, and the current–voltage curve was linear over the entire voltage range. This membrane current pattern is characteristic for astrocytes (Steinhäuser et al., 1994).

We did not observe a Ca^{2+} increase in all X-Rhod-labeled cells in response to CSD, which is most likely attributable to the much lower sensitivity and worse signal-to-noise ratio of X-Rhod compared with Fluo-4. Fluo-4, on the other hand, could not be combined with EGFP fluorescence because of the overlap of the spectra, but, because of its better sensitivity, we used this dye in nontransgenic animals for all additional experiments. To characterize the population of Fluo-4-labeled cells, we used the patch-clamp protocol as described above: all Fluo-4-loaded cells had the same, astrocyte-like current pattern as the X-Rhod-labeled cells from the transgenic animals ($n = 25$ from $n = 19$ slices) (Fig. 1*C*). In a third approach, we also tested the ability of the stained cells to react with a Ca^{2+} signal during low K^+, another method to identify astrocytes *in situ* (Dallwig and Deitmer, 2002), and found that, on average, approximately two of three stained cells responded to low external K^+ concentrations ($n = 60$ from $n = 3$ slices). We can conclude that the dye-loaded cells in neocortical slices from P10–P14 mice are almost exclusively astrocytes. In additional experiments, we bulk loaded slices from adult mice (P28–P36) with Fluo-4 using the same protocol as used for the juvenile tissue. The principal findings were well comparable: cells showed spontaneous Ca^{2+} spikes when superfusion in the submerged chamber was halted (see also below), whereas during CSD, numerous single cells responded with Ca^{2+} increases appearing as a wave-like phenomenon. Because less cells were stained in adult slices and the signal-to-noise ratio in these experiments was significantly lower compared with the fluorescence changes in slices from juvenile mice, we performed all additional experiments using P10–P14 slices.

The astrocyte Ca^{2+} wave and the depolarization spread in the first instance in synchrony

We used two techniques to record CSD, extracellular DC-potential recordings with microelectrodes and imaging of the IOS. The latter corresponds to changes in light scattering partly caused by alterations of the extracellular space volume (Holthoff and Witte, 1996). Recording IOS permits two-dimensional mapping of the spreading event with limited time resolution, whereas electrodes can register the voltage changes only from a limited number of points, but with a high time resolution (Somjen, 2001). To compare the spread of the astrocytic Ca^{2+} wave and IOS over larger areas, we used a low magnification (10× objective) in which individual astrocytes could still be recognized but not their subcellular morphology. To analyze the spread of the astrocytic Ca^{2+} wave, we subtracted the control image (image taken before stimulation) from any given image: thus, only those cells were highlighted that responded to CSD with an increase in intracellular Ca^{2+} (Fig. 2*A*). In the same way, we analyzed the IOS by subtracting the control from the images. Figure 2*A* illustrates that the Ca^{2+} signal and IOS spread with a similar velocity through the tissue. The IOS spreads with a delay: usually the onset of the first bright signal of the IOS (named part b by the Brazilian school) (for review, see Somjen, 2001) occurred within one image delay compared with the Ca^{2+} signal (image sampling interval was 2.3 sec). The frontline of the bright signal of the IOS was ~100 μm behind the Ca^{2+} signal.

To get a better temporal relationship between cortical spreading depression and the Ca^{2+} signal, we recorded the extracellular potential with microelectrodes. The tip of a pipette was placed close to a dye-loaded cell. This allowed us to get a temporal correlation between the increase in intracellular Ca^{2+} of one single astrocyte, the IOS (measured from the same region of interest), and the field potential. As shown in Figure 2*B* and with a higher temporal resolution in Figure 2*C*, the Ca^{2+} and field potential changes occurred synchronously, whereas the IOS appeared with a substantial delay.

Astrocyte Ca^{2+} waves spread farther than CSD

The IOS typically spread for ~1 mm in our model and then rapidly decayed within ~200 μm (Figs. 3*A*, 4, IOS traces). This correlates well with the negative DC-potential shifts recorded with extracellular electrodes. Detectable DC signals (>1 mV) were only observed in areas in which IOS could be recorded. When IOS decayed with increasing distance (Figs. 3*A*, 4), the DC-potential shift also disappeared. In contrast, astrocyte Ca^{2+} responses could be recorded at a distance of up to 1.5 mm from the point of stimulation and thus in regions without IOS (Figs. 3*B*, 4). In the core area, in which both astrocyte Ca^{2+} waves and IOS could be recorded, both signals spread with comparable speed, namely with 39.2 ± 3.3 μm/sec ($n = 62$ from $n = 8$ slices). Moreover, in this region, the astrocytic Ca^{2+} response was accompanied by an inward current reflecting the depolarization of the cell as investigated by using the patch-clamp technique and filling the cell with the Ca^{2+}-sensitive dye via the pipette (Fig. 5*A*). In peripheral areas in which IOS was no longer detectable, the astrocytic Ca^{2+} increase was not accompanied by a detectable membrane current, and thus the astrocyte did not depolarize (Fig. 5*B*). Thus, the astrocytic Ca^{2+} wave spreads farther than the cortical spreading depression as measured by IOS and confirmed by electrophysiological measurements. Moreover, the astrocytic

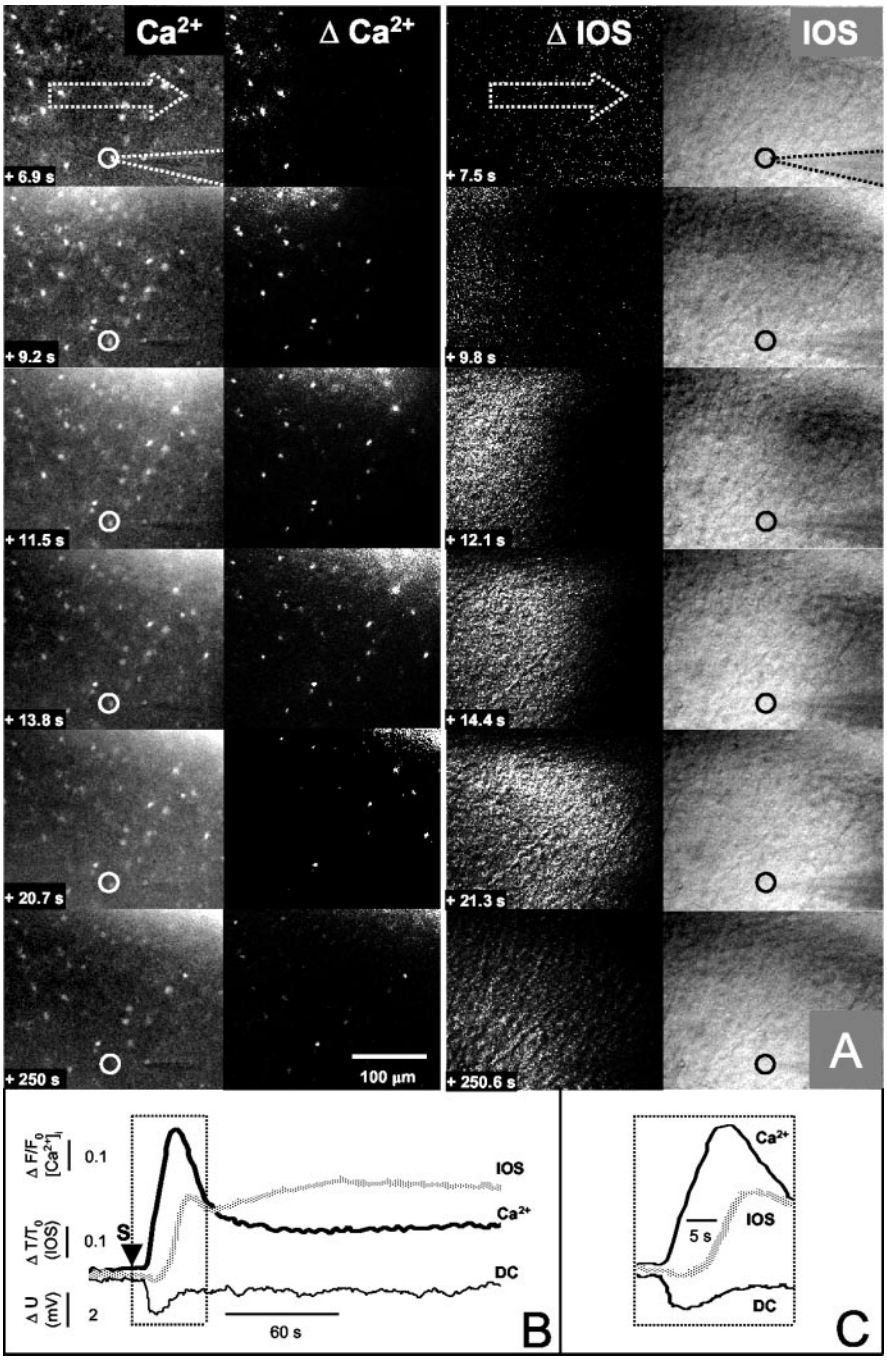

Figure 2. Correlation of DC-potential shift, astrocytic Ca^{2+} increases, and IOS. *A*, A sequence of fluorescence images displaying changes in Ca^{2+} (left columns) and corresponding IOS (right columns) were recorded with low magnification (10×). Fluo-4 fluorescence is displayed as contrast-enhanced images (Ca^{2+}) or as images in which the background (i.e., image before stimulation) was subtracted (ΔCa^{2+}). In the same manner, the IOS and ΔIOS are displayed on the right and were recorded with a delay to the fluorescence signal of 600 msec. As indicated by the white dotted arrows in the first rows, CSD spread from the left to the right. Note that the frontlines of the astrocytic Ca^{2+} wave spread ~100 μm ahead of IOS changes. The time in the left bottom corner of each picture indicates time after stimulation. *B*, A DC pipette was placed close to a stained astrocyte (as indicated in the first images; dotted lines refer to the extracellular recording electrode, and the circle denotes the region of interest from which fluorescence and light transmittance were recorded). The arrow (S) indicates the time of KCl ejection. Background-subtracted fluorescence signal corresponding to changes in Ca^{2+} ($\Delta F/F_0$), IOS ($\Delta T/T_0$), and the DC potential (ΔU) are displayed. *C*, Trace in *B* with higher time resolution. Whereas the onset of the Ca^{2+} increase and negative DC-potential shift occurred simultaneously, the IOS signal occurred with a delay of 5–8 sec.

Ca^{2+} wave changed its properties in the periphery: (1) the astrocyte Ca^{2+} wave was slower and spread with a speed of 18.3 ± 2.5 μm/sec (n = 38 cells from n = 8 slices), thus approximately one-half of the speed when associated with IOS (Fig. 3); and (2) the Ca^{2+} response typically consisted of two or more successive peaks (Figs. 4, 5*B*; velocity was always determined by comparing the first peaks after stimulation).

The NMDA-antagonist MK-801 blocks CSD but not the astrocyte Ca^{2+} wave

The NMDA-receptor antagonist MK-801 is known to prevent CSD *in vivo* (Jander et al., 2001) and *in vitro* (Basarsky et al., 1999). We applied MK-801 (40 μM) for at least 10 min before KCl was ejected from the micropipette to trigger CSD. Under these conditions, in a distance of ~300 μm and more from the ejection side, changes in IOS (Fig. 6*B*) and DC-potential shifts were not detected. In contrast, the astrocyte Ca^{2+} wave was still recorded (Fig. 6*A*), but the time course of the Ca^{2+} change was different compared with control: there was a small, rapid increase to a sustained plateau, and the characteristic transient Ca^{2+} increase, typically associated with the Ca^{2+} wave, occurred with a delay. This resulted in a reduced velocity of propagation of the wave (13.2 ± 1.5 μm/sec; n = 20 cells from n = 4 slices), well comparable with the speed of the astrocyte Ca^{2+} signal found in the periphery of CSD and astrocyte culture. During washout of the NMDA blocker, the astrocyte Ca^{2+} wave propagated as rapidly as in the control before MK-801 application, although IOS (Fig. 6*A*) and DC-potential shift did not completely recover.

The specific gap junction blocker carbenoxolon does not alter the spread of CSD but decelerates the astrocyte Ca^{2+} wave in the periphery of CSD

Numerous gap junction blockers have been shown to prevent CSD (Nedergaard et al., 1995). We tested the effect of the specific gap junction blocker carbenoxolon on CSD and the astrocyte Ca^{2+} wave. Carbenoxolon (100 μM) was applied for at least 10 min before CSD was triggered. The gap junction blocker did neither prevent CSD nor blocked the astrocyte Ca^{2+} signal coupled to depolarization. In contrast, the "intrinsic" astrocyte Ca^{2+} wave in the periphery, uncoupled to depolarization, was substantially altered. Approximately one of three astrocytes no longer participated in the Ca^{2+} wave. Within the remaining population of cells, the speed of the spread was decelerated to 2.9 ± 0.9 μm/sec (n = 18 cells from n = 4 slices).

Ca^{2+} increases synchronously in adjacent neurons and astrocytes in response to CSD

To compare the glial response during CSD with that of neurons, we recorded membrane currents and intracellular Ca^{2+} signals

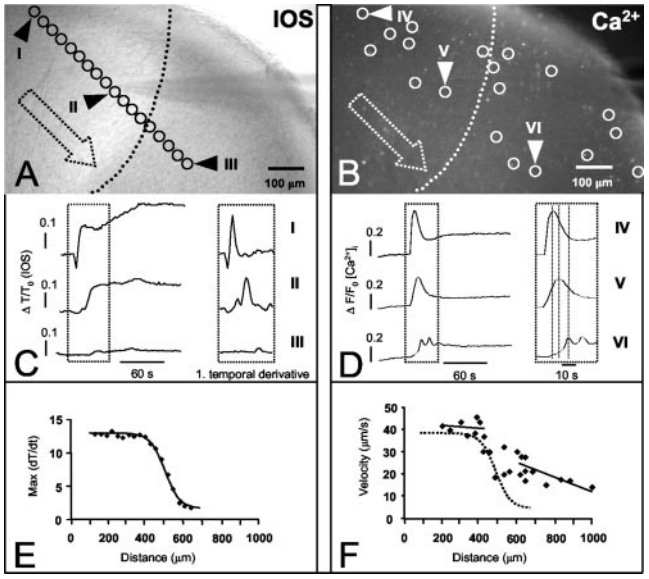

Figure 3. Astrocytic Ca^{2+} signals spread farther than IOS. *A*, *B*, IOS (*A*) and Fluo-4 fluorescence correlated to Ca^{2+} signals (*B*) were studied in a cortical slice. The circles define the regions of interest from which IOS and fluorescence signals were recorded as a function of distance from the stimulation pipette. The arrow denotes the direction in which the signals spread. The dotted line indicates how far the IOS spreads. *C*, The three traces on the left display the background-corrected IOS ($\Delta T/T_0$) at the three regions indicated in *A*. The traces on the right show the first derivative, which represents a better measure of the IOS strength than the amplitude. *D*, The three traces display the background corrected changes in Ca^{2+} ($\Delta F/F_0$) at the three regions indicated in *B*. The traces on the left are shown in an expanded time scale to better illustrate the delays in the peak. *E*, The amplitude of the first derivative of the IOS [Max (dT/dt)] was plotted as a function of distance to the stimulation pipette. Note the decline in the IOS at ~500 μm. The data points were fitted by a two-exponential function. *F*, The velocity of the Ca^{2+} wave was determined by measuring the time between Ca^{2+} peaks of two closely apposed fluorescent cells and was plotted as a function of distance from the stimulation pipette. The dotted line indicates the fit in *E*. Velocity values between 0 and 450 μm (40.9 $\pm$ 3.2 μm/sec; 80–100% of IOS) and 600 and 1100 μm (20.7 $\pm$ 5.5 μm/sec; 0–20% of the IOS) were fitted. The fits thus indicate the two different speeds of the astrocytic Ca^{2+} wave in the core area and the peripheral zone.

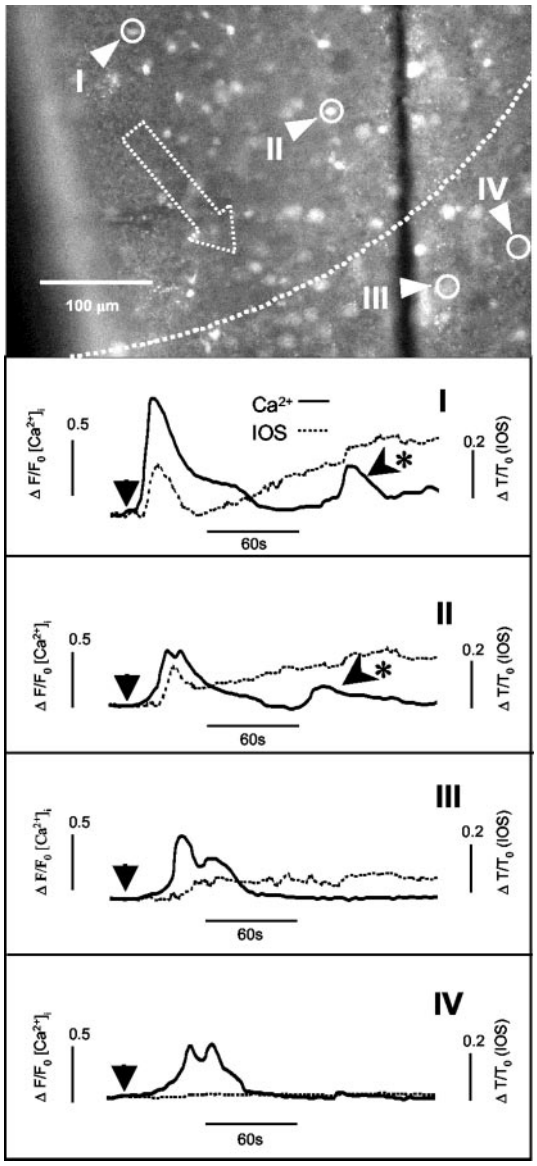

Figure 4. Ca^{2+} signals of single astrocytes and the corresponding IOS in the core versus the periphery. Similar as described in Figure 3, fluorescence changes (F/F_0) from four different astrocytes and the corresponding IOS ($\Delta T/T_0$) were recorded. This region was selected because it contained the zone in which the IOS signal decayed (indicated by the dotted line), and it is shown in higher magnification as in Figure 3. On the top, the fluorescence image is shown with the selected cells indicated by circles and labeled by Roman numbers. Below are the responses of the four different cells. Note the occurrence of spontaneous astrocytic Ca^{2+} activity (arrow with an asterisk; cells I and II).

from a neuron close (<20 μm apart) to a bulk-loaded glial cell ($n = 5$ from $n = 5$ slices) (Fig. 7). The neuron was dye-loaded via the pipette for 20–30 min. When the perfusion was switched off, a small inward current and an increase in spontaneous postsynaptic currents was observed in the neuron, whereas spontaneous Ca^{2+} spikes were recorded in the astrocyte. In a few cases, when the neuron and glial cell were closely apposed, synchronized spontaneous Ca^{2+} spikes were recorded from both types of cells (Fig. 7). After initiation of CSD by application of KCl, a synchronous Ca^{2+} increase was recorded in both neuron and astrocyte.

Spontaneous Ca^{2+} activity in astrocytes is absent after the wave has passed

Before we ejected KCl to trigger CSD, we switched off the bath perfusion. This led to a consistent effect: many of the dye-loaded cells responded with spontaneous Ca^{2+} oscillations. The procedure, namely switching off the perfusion, also allowed us to identify the dye-loaded astrocytes. This response pattern was observed in bulk-loaded (Fig. 7) but not in patched astrocytes. All spontaneously active cells responded with a Ca^{2+} increase during CSD. Immediately after CSD, however, no spontaneous Ca^{2+} activity was observed in previously active astrocytes. Then, beginning ~60–80 sec after the Ca^{2+} peak, the spontaneous Ca^{2+} activity started to recover (Figs. 4, 8, arrows with an asterisk).

Strong reduction in intracellular astrocytic Ca^{2+} signaling by depletion of internal Ca^{2+} stores does not affect the propagation of the IOS

Two paradigms were found to block both phenomena (the astrocytic Ca^{2+} wave and CSD) completely: application of the gap junction blocker octanol (500 μM; $n = 4$) and washing the slice in Ca^{2+} free buffer for at least 5 min (2 mM EGTA; $n = 4$). To elucidate whether IOS could propagate when internal astrocytic Ca^{2+} stores are depleted, we conducted the following series of experiments. After a control measurement (Fig. 8*A*), we used a standard paradigm to deplete intracellular Ca^{2+} stores: thapsigargin, which is known to prevent the reuptake of calcium into internal stores (Lytton et al., 1991), was added to the buffer solution (500 nM) for 10 min. Then, ATP (10 μM) was applied for 1

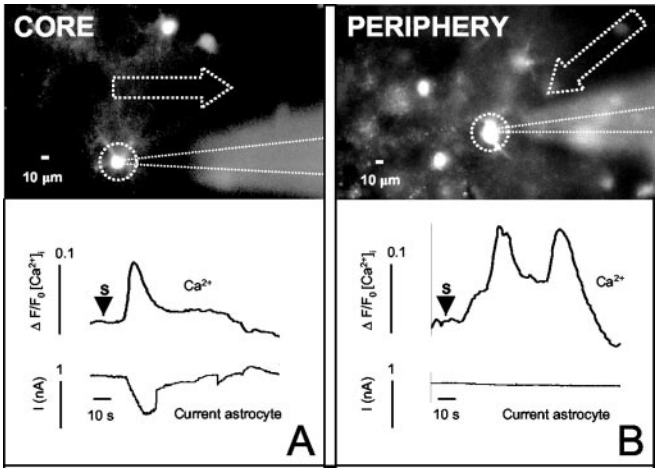

Figure 5. Astrocytic membrane currents can only be detected in the core of CSD. *A*, Membrane currents (*I*) and $\Delta F/F_0$ were recorded from an astrocyte identified by its current pattern. The cell was selected close to the stimulation pipette, and the direction of the wave is indicated by an arrow. Note the inward current in response to stimulation (S). *B*, With a similar paradigm as described in *A*, current and Ca^{2+} responses were recorded from an astrocyte distant to the stimulation pipette. While a Ca^{2+} signal was recorded, no change in membrane current was observed. Note the biphasic Ca^{2+} response typical for cells in the periphery.

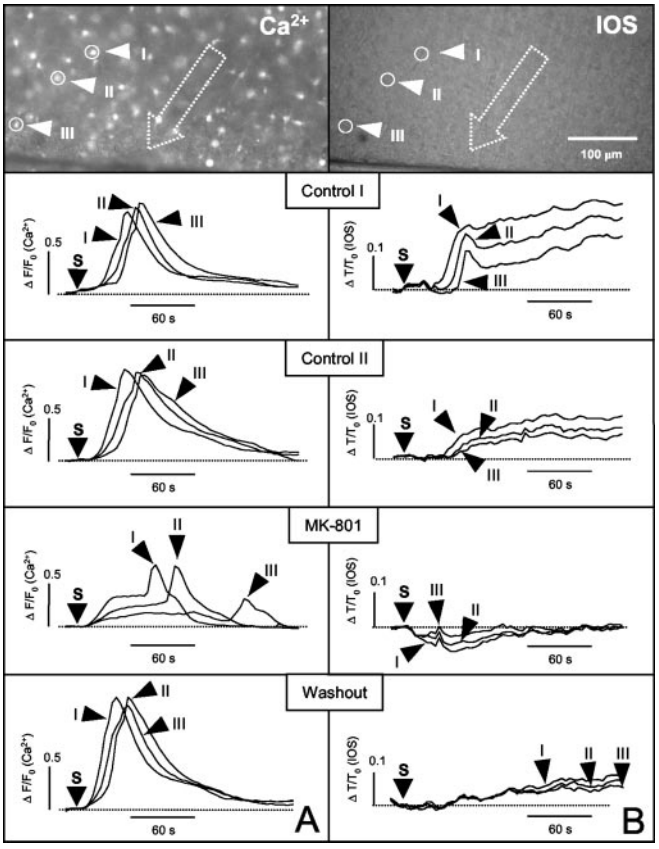

Figure 6. MK-801 blocks CSD and decelerates the astrocyte Ca^{2+} wave. Two control experiments were performed before MK-801 was applied. Repeatedly triggered CSDs induced reproducible Ca^{2+} increases in astrocytes. Characteristically, the IOS lost the four-phasic shape, when CSD was triggered many times in short intervals, although negative DC shifts remained comparable. The NMDA receptor blocker MK-801 prevented CSD. In contrast, an astrocytic Ca^{2+} wave with a significantly lowered speed, preceded by a rapid increase to a sustained plateau, was still detectable. During washout, the astrocytic Ca^{2+} signals were restored, although IOS changes did not indicate a complete recovery of the CSD. S, Stimulation.

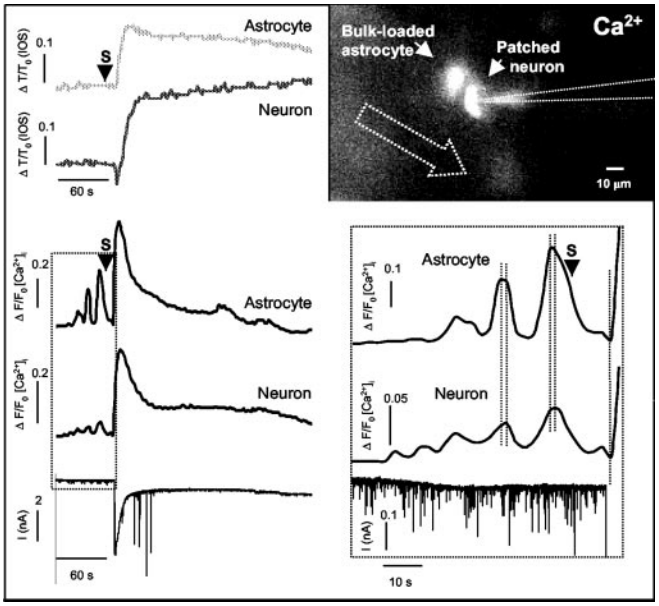

Figure 7. Ca^{2+} responses of a closely apposed neuron and astrocyte during CSD. A neuron in close proximity to a bulk-loaded astrocyte was selected for patch clamping (fluorescence image on the top right). The patch pipette was filled with Fluo-4 salt to load the neuron with the Ca^{2+} sensor. This allowed us to record Ca^{2+} responses ($\Delta F/F_0$) from the neuron and the astrocyte and current (*I*) from the neuron and IOS ($\Delta T/T_0$) at the region of interest selected for neuron and astrocyte ($\Delta T/T_0$). Time of KCl ejection (S, stimulation) is indicated by an arrow. The perfusion was switched off 60 sec before stimulation. Note the increasing spontaneous Ca^{2+} activity in both cells. The traces on the right with an expanded time scale illustrate the synchronous Ca^{2+} activity of the neuron and the astrocyte. The vertical lines indicate the Ca^{2+} peaks.

min, which triggered a Ca^{2+} response. A second response to ATP could not longer be elicited, indicating that this procedure had led to a complete depletion of the stores. Moreover, cells, which had shown previously spontaneous Ca^{2+} activity, were silent. When CSD was initiated after depletion of internal Ca^{2+} stores, the Ca^{2+} wave in astrocytes could still be recorded, but the amplitude of the Ca^{2+} signal was markedly reduced ($n = 28$ from $n = 3$ slices) (Fig. 8*B*,*C*). In contrast, the IOS was still recorded and did not show significant changes compared with control conditions. To ensure the best possible recovery of the IOS, the second stimulation was initiated 1 hr after the first one in this sequence of experiments. We conclude that the release of Ca^{2+} from internal stores in astrocytes is not required for the propagation of CSD.

Discussion

In this study, we visualized intracellular Ca^{2+} signaling in a large population of neocortical astrocytes during CSD in acute slices from mice. Our data reveal a complex relationship, in which CSD in the first instance determines the velocity of an accompanying astrocytic Ca^{2+} wave until the spread of depolarization decays. However, the astrocytic Ca^{2+} wave moves on and propagates as a self-reliant mechanism, which covers a larger territory, but spreads with a lower velocity. By selectively inducing only astrocyte Ca^{2+} waves or CSD using pharmacological tools, different mechanisms of propagation become obvious.

Glial Ca^{2+} waves *in vitro* and *in situ*

Astrocyte Ca^{2+} waves have been reported in culture (Cornell-Bell et al., 1990; Dani et al., 1992) and have also been observed recently *in situ*, namely in the retina (Newman and Zahs, 1997)

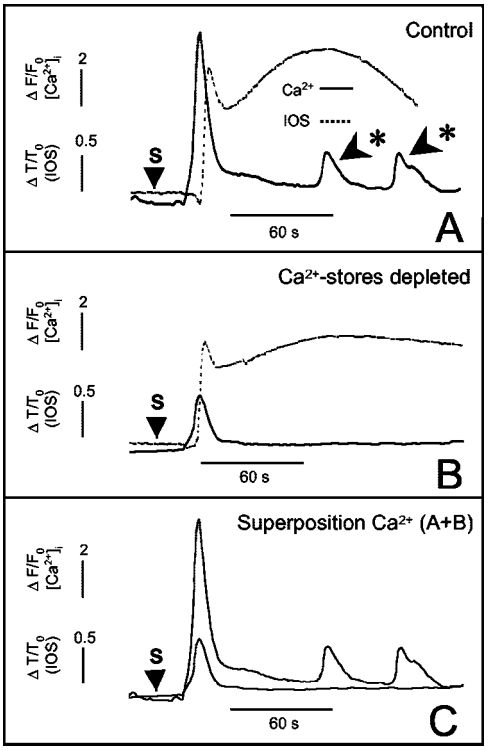

Figure 8. Depletion of internal Ca^{2+} stores does not influence the spread of IOS. *A*, *B*, A Ca^{2+} response ($\Delta F/F_0$) and IOS ($\Delta T/T_0$) were recorded from an astrocyte in response to KCl stimulation (*S*) before (*A*, control) and after (*B*) Ca^{2+} stores were depleted. To deplete stores, thapsigargin was added for 10 min, and subsequently ATP was applied for 1 min. The second response was elicited 60 min after the control. *C*, Superposition of the Ca^{2+} responses from *A* and *B*. Note the occurrence of spontaneous astrocytic Ca^{2+} activity (arrows with an asterisk).

and in the corpus callosum (Schipke et al., 2002), but their pathophysiological occurrence and impact are still unknown. Studies performed in hippocampal tissues revealed that Ca^{2+} waves, which could not unequivocally be attributed to a certain cell type but in which single astrocytes have been shown to participate, appear during spreading depression (Basarsky et al., 1998; Kunkler and Kraig, 1998). Given the widespread potential signaling capacities of cytosolic Ca^{2+} increases (Nedergaard, 1994; Parpura et al., 1994; Pasti et al., 1997; Parri et al., 2001), it has been suggested that astrocytic Ca^{2+} signals may play a pivotal role in CSD (Martins-Ferreira et al., 2000).

We used the bulk-loading technique to fill cells in neocortical slices from mice with the Ca^{2+} dyes X-Rhod or Fluo-4. When superfusion in the submerged chamber was stopped, spontaneous Ca^{2+} oscillations occurred, which disappeared after restarting the flow. We speculate that unknown factors are chronically released into the extracellular space and activate spontaneous Ca^{2+} activity. We assume that these factors are washed out when the slices are superfused.

Ca^{2+} dyes label a defined population of cells

In a first approach to characterize the stained cells, we used a transgenic animal in which EGFP expression is under the control of the GFAP promoter, and thus astrocytes are labeled with the green fluorescent protein (Nolte et al., 2001). EGFP- and X-Rhod-stained cell populations overlap but only partially, and this reflects the observation that, particularly in the cortex, most cells with astrocyte morphology are GFAP negative (Kalman and Hajos, 1989). For this reason, we used the patch-clamp technique to further characterize the dye-loaded cells. Without exception, all stained and patch-clamped cells exhibited the typical membrane current pattern of astrocytes, which is distinct from neurons, oligodendrocytes, glial progenitor cells, and microglia (Berger et al., 1991; Steinhäuser et al., 1994; Boucsein et al., 2000). In a third approach to identify the dye-loaded cells, we tested Ca^{2+} responses during low extracellular K^+ concentration, because it was reported recently that this stimulus induces Ca^{2+} increases in astrocytes selectively (Dallwig and Deitmer, 2002). We also applied this paradigm and found that approximately two of three dye-labeled and spontaneous oscillating cells reacted during the low K^+ stimulus. The selective loading of astrocytes also depends on the developmental state of the brain: in young mice up to P5, both neurons and astrocytes take up the dye (our unpublished observation), but in contrast, in older animals, only astrocytes are stained. We conclude that, in our conditions, the bulk-loading procedure labels a defined population of cells, which express the electrophysiological features of astrocytes, although not all of them are GFAP labeled.

CSD triggers an astrocyte Ca^{2+} wave in young and adult animals

The two-dimensional spread of CSD depends on the cytoarchitecture, the volume of the interstitial space, and the developmental state. SD has so far only been observed in animals older than P10, and, in some brain regions, SD can even only be elicited after P25 (Somjen, 2001). We also observed Ca^{2+} oscillations and waves with single-cell resolution in slices prepared from adult mice, but because of the significantly better staining, we performed most experiments using slices from juvenile mice (P10–P14). We found that slices of this age allow both selective bulk-loading of astrocytes with an excellent signal-to-noise ratio and reliable CSD elicitation by KCl ejection. When we induced CSD in the submerged chamber, it usually spread over a distance of up to 1 mm as measured by IOS, whereas in older animals, SD in the neocortex spreads within larger areas of the ipsilateral hemisphere (Vilagi et al., 2001; Anderson and Andrew, 2002; our unpublished observations). Notably, when the slices in our study were in a bad shape, after being kept in the submerged chamber for several hours, CSD occasionally also spread farther. We did not modify the extracellular solution as done in a previous study to extent the two-dimensional spread in healthy slices (Basarsky et al., 1998; Kunkler and Kraig, 1998), because we found that even minor modifications, like reducing or enhancing K^+, influenced astrocyte Ca^{2+} signals. Interestingly, in a model using human brain slices, KCl-induced CSD is also restricted to a rather small brain area (Gorji et al., 2001; Dr. A, Gorji, personal communication). We feel that our model mimics the situation in the human brain.

Astrocyte Ca^{2+} signals are not essential for the propagation of CSD

We found that the astrocyte Ca^{2+} wave and membrane depolarization occur in synchrony. Basarsky et al. (1998) measured SD in the hippocampus and reported that the Ca^{2+} signal propagated many seconds ahead of the IOS. We also observed this delay in the IOS, but simultaneous measurements of extracellular field potentials or neuronal responses, such as changes in membrane currents or intracellular $[Ca^{2+}]$, occurred in synchrony with the astrocytic response. We therefore conclude that the astrocyte Ca^{2+} wave in slices of neocortical tissue is not a leading signal in CSD propagation. Contrasting results were reported in hip-

pocampal organ cultures, in which two types of Ca^{2+} waves, a fast one most likely of neuronal origin and a slower wave, occur during spreading depression (Kunkler and Kraig, 1998). Even the slower one, which was attributed to astrocytes, preceded the DC-potential shift by several seconds.

In the hippocampus, it has been observed that the propagation of CSD is not altered in low [Ca^{2+}], whereas Ca^{2+} signals from astrocytes could not longer be detected (Basarsky et al., 1998). In contrast, in hippocampal cultures, attempts to separate spreading depression and accompanying Ca^{2+} waves were not successful (Kunkler and Kraig, 1998). We were unable, like others (Nedergaard et al., 1995; Martins-Ferreira et al., 2000), to induce CSD in low extracellular [Ca^{2+}]. To eliminate inter-astrocytic Ca^{2+} signaling, we chose to deplete internal Ca^{2+} stores. Our data indicate that release of Ca^{2+} from internal stores is not essential for the spread of CSD: depletion of intracellular Ca^{2+} pools does not alter the two-dimensional propagation of CSD, whereas the astrocyte Ca^{2+} wave was blocked.

Different mechanisms underlie propagation of CSD and astrocyte Ca^{2+} waves

We found that CSD has an impact on the accompanying glial Ca^{2+} wave, but the astrocyte signal penetrates a larger brain volume. In concert with CSD, the glial response propagates with the speed of CSD, namely in the range of 30–50 μm/sec. After the wave has propagated to the periphery where CSD has decayed or when CSD is blocked by MK-801, the glial Ca^{2+} response spreads with a lower speed (10–20 μm/sec), which matches the velocity of Ca^{2+} signals in cultured astrocytes (Cornell-Bell et al., 1990) or in white matter (Schipke et al., 2002). This indicates that CSD drives the glial signaling to propagate with a higher speed. We conclude that astrocyte Ca^{2+} waves are sustained by (at least) two different mechanisms: one is driven by CSD, and another one is controlled by intrinsic astrocyte activity. The intrinsic astrocyte wave is not affected by the NMDA antagonist MK-801 and can thus be separated from CSD. Inter-astrocytic communication in the periphery of CSD could be mediated by diffusion of second messengers through gap junctions (Giaume and Venance, 1998) or the release of substances into the extracellular space (Guthrie et al., 1999; Schipke et al., 2002). Although gap junctions have been discussed to play a pivotal role in the propagation of CSD (Nedergaard et al., 1995; Martins-Ferreira et al., 2000), our data indicate that the selective gap junction blocker carbenoxolon does not affect CSD or the astrocyte wave associated with depolarization. This is in good agreement with the recent finding that CSD is accelerated in mice with astrocyte-directed inactivation of connexin 43, the major gap junction protein of astrocytes (Theis et al., 2003). However, the gap junction blocker carbenoxolon has a pronounced decelerating effect on the intrinsic astrocytic Ca^{2+} wave in the periphery of CSD.

References

Anderson TR, Andrew RD (2002) Spreading depression: imaging and blockade in the rat neocortical brain slice. J Neurophysiol 88:2713–2725.

Araque A, Carmignoto G, Haydon PG (2001) Dynamic signaling between astrocytes and neurons. Annu Rev Physiol 63:795–813.

Back T, Ginsberg MD, Dietrich WD, Watson BD (1996) Induction of spreading depression in the ischemic hemisphere following experimental middle cerebral artery occlusion: effect on infarct morphology. J Cereb Blood Flow Metab 16:202–213.

Basarsky TA, Duffy SN, Andrew RD, MacVicar BA (1998) Imaging spreading depression and associated intracellular calcium waves in brain slices. J Neurosci 18:7189–7199.

Basarsky TA, Feighan D, MacVicar BA (1999) Glutamate release through volume-activated channels during spreading depression. J Neurosci 19:6439–6445.

Berger T, Schnitzer J, Kettenmann H (1991) Developmental changes in the membrane current pattern, K^+ buffer capacity, and morphology of glial cells in the corpus callosum slice. J Neurosci 11:3008–3024.

Boucsein C, Kettenmann H, Nolte C (2000) Electrophysiological properties of microglial cells in normal and pathologic rat brain slices. Eur J Neurosci 12:2049–2058.

Charles A (1998) Intercellular calcium waves in glia. Glia 24:39–49.

Cornell-Bell AH, Finkbeiner SM, Cooper MS, Smith SJ (1990) Glutamate induces calcium waves in cultured astrocytes: long-range glial signaling. Science 247:470–473.

Cotrina ML, Lin JH, Lopez-Garcia JC, Naus CC, Nedergaard M (2000) ATP-mediated glia signaling. J Neurosci 20:2835–2844.

Dallwig R, Deitmer JW (2002) Cell-type specific calcium responses in acute rat hippocampal slices. J Neurosci Methods 116:77–87.

Dani JW, Chernjavsky A, Smith SJ (1992) Neuronal activity triggers calcium waves in hippocampal astrocyte networks. Neuron 8:429–440.

Giaume C, Venance L (1998) Intercellular calcium signaling and gap junctional communication in astrocytes. Glia 24:50–64.

Gorji A (2001) Spreading depression: a review of the clinical relevance. Brain Res Rev 38:33–60.

Gorji A, Scheller D, Straub H, Tegtmeier F, Kohling R, Hohling JM, Tuxhorn I, Ebner A, Wolf P, Werner PH, Oppel F, Speckmann EJ (2001) Spreading depression in human neocortical slices. Brain Res 906:74–83.

Guthrie PB, Knappenberger J, Segal M, Bennett MV, Charles AC, Kater SB (1999) ATP released from astrocytes mediates glial calcium waves. J Neurosci 19:520–528.

Hadjikhani N, Sanchez DR, Wu O, Schwartz D, Bakker D, Fischl B, Kwong KK, Cutrer FM, Rosen BR, Tootell RB, Sorensen AG, Moskowitz MA (2001) Mechanisms of migraine aura revealed by functional MRI in human visual cortex. Proc Natl Acad Sci USA 98:4687–4692.

Holthoff K, Witte OW (1996) Intrinsic optical signals in rat neocortical slices measured with near-infrared dark-field microscopy reveal changes in extracellular space. J Neurosci 16:2740–2749.

Iijima T, Mies G, Hossmann KA (1992) Repeated negative DC deflections in rat cortex following middle cerebral artery occlusion are abolished by MK-801: effect on volume of ischemic injury. J Cereb Blood Flow Metab 12:727–733.

Jander S, Schroeter M, Peters O, Witte OW, Stoll G (2001) Cortical spreading depression induces proinflammatory cytokine gene expression in the rat brain. J Cereb Blood Flow Metab 21:218–225.

Kalman M, Hajos F (1989) Distribution of glial fibrillary acidic protein (GFAP)-immunoreactive astrocytes in the rat brain. I. Forebrain. Exp Brain Res 8:147–163.

Kunkler PE, Kraig RP (1998) Calcium waves precede electrophysiological changes of spreading depression in hippocampal organ cultures. J Neurosci 18:3416–3425.

Lauritzen M (1994) Pathophysiology of the migraine aura. The spreading depression theory. Brain 117:199–210.

Leao AAP (1944) Spreading depression of activity in the cerebral cortex. J Neurophysiol 7:359–390.

Lytton J, Westlin M, Hanley MR (1991) Thapsigargin inhibits the sarcoplasmic or endoplasmic reticulum Ca-ATPase family of calcium pumps. J Biol Chem 266:17067–17071.

Martins-Ferreira H, Nedergaard M, Nicholson C (2000) Perspectives on spreading depression. Brain Res Brain Res Rev 32:215–234.

Nedergaard M (1994) Direct signaling from astrocytes to neurons in cultures of mammalian brain cells. Science 263:1768–1771.

Nedergaard M, Cooper AJ, Goldman SA (1995) Gap junctions are required for the propagation of spreading depression. J Neurobiol 28:433–444.

Newman EA, Zahs KR (1997) Calcium waves in retinal glial cells. Science 275:844–847.

Nolte C, Matyash M, Pivneva T, Schipke CG, Ohlemeyer C, Hanisch UK, Kirchhoff F, Kettenmann H (2001) GFAP promoter-controlled EGFP-expressing transgenic mice: a tool to visualize astrocytes and astrogliosis in living brain tissue. Glia 33:72–86.

Parpura V, Basarsky TA, Liu F, Jeftinija K, Jeftinija S, Haydon PG (1994) Glutamate-mediated astrocyte-neuron signalling. Nature 369:744–747.

Parri HR, Gould TM, Crunelli V (2001) Spontaneous astrocytic Ca^{2+} oscillations in situ drive NMDAR-mediated neuronal excitation. Nat Neurosci 4:803–812.

Pasti L, Volterra A, Pozzan T, Carmignoto G (1997) Intracellular calcium oscillations in astrocytes: a highly plastic, bidirectional form of communication between neurons and astrocytes *in situ*. J Neurosci 17:7817–7830.

Schipke CG, Boucsein C, Ohlemeyer C, Kirchhoff F, Kettenmann H (2002) Astrocyte Ca^{2+} waves trigger responses in microglial cells in brain slices. FASEB J 16:255–257.

Somjen GG (2001) Mechanisms of spreading depression and hypoxic spreading depression-like depolarization. Physiol Rev 81:1065–1096.

Steinhäuser C, Jabs R, Kettenmann H (1994) Properties of GABA and glutamate responses in identified glial cells of the mouse hippocampal slice. Hippocampus 4:19–35.

Stout CE, Costantin JL, Naus CC, Charles AC (2002) Intercellular calcium signaling in astrocytes via ATP release through connexin hemichannels. J Biol Chem 277:10482–10488.

Theis M, Jauch R, Zhuo L, Speidel D, Wallraff A, Doring B, Frisch C, Sohl G, Teubner B, Euwens C, Huston J, Steinhäuser C, Messing A, Heinemann U, Willecke K (2003) Accelerated hippocampal spreading depression and enhanced locomotory activity in mice with astrocyte-directed inactivation of connexin43. J Neurosci 23:766–776.

Verkhratsky A, Kettenmann H (1996) Calcium signalling in glial cells. Trends Neurosci 19:346–352.

Vilagi I, Klapka N, Luhmann HJ (2001) Optical recording of spreading depression in rat neocortical slices. Brain Res 898:288–296.